Journal of the Meteorological Society of Japan

EARLY ONLINE RELEASE

The DOI for this manuscript is
DOI:10.2151/jmsj.2023-008
J-STAGE Advance published date: November 17th, 2022

What is the equivalent depth of the Pekeris mode?

Keiichi Ishioka

Graduate School of Science, Kyoto University

Corresponding author: Keiichi Ishioka, Graduate School of Science, Kyoto University, Kitashirakawa-Oiwake-cho, Sakyo-ku, Kyoto 606-8502, Japan.
E-mail: ishioka@gfd-dennou.org

Abstract

Inspired by the detection of the Pekeris mode of atmospheric free oscillations by a recent study, high-accuracy numerical calculations of the problem of determining the equivalent depth of atmospheric free oscillations are performed. Here, the computational method is largely based on a previous study, but with modifications to improve the accuracy of the calculation. Two equivalent depths are found, with values of 9.9 km and 6.6 km. The former corresponds to the Lamb mode and the latter corresponds to the Pekeris mode. These values deviate from those obtained in the previous study, especially for the Pekeris mode. The causes of this discrepancy is discussed, as well as the correspondence between the equivalent depths obtained in this study and that of the Pekeris mode detected in the recent study.

1. Introduction

The explosive eruption of the Hunga Tonga-Hunga Ha'apai volcano on January 15, 2022 is the largest eruption since the development of the modern global observation network of the Earth and has had a significant impact on various fields of earth science. One such prominent example is the first detection of the Pekeris mode by Watanabe, et al. (2022).

The Pekeris mode was theoretically predicted by Pekeris (1937) as a free oscillation mode with solving the vertical structure equation of the atmospheric tidal theory for various temperature profiles of the atmosphere, which were considered realistic at that time. Pekeris (1937) showed that a mode with the equivalent depth of about 8 km could exist as a different mode from the Lamb mode. A detailed calculation of the vertical structure equation giving a more realistic temperature structure of the atmosphere, U.S. Standard Atmosphere, 1976 (NOAA, et al., 1976), which we cite as USSA76, was later performed by Salby (1979). There, the existence of a mode with the equivalent depth of 9.6 km and a mode with the equivalent depth of 5.8 km were suggested. The former corresponds to the Lamb mode and the latter corresponds to the Pekeris mode, which Salby (1979) named as "the ducted mode". Whereas the Lamb mode has been detected in many studies (see Sakazaki and Hamilton, 2020, and references therein), the Pekeris mode has not been detected until Watanabe, et al. (2022). In Watanabe, et al. (2022), they analyzed radiance observations taken from the Himawari-8 geostationary satellite and showed that two distinct wave fronts were detected, the phase speeds of which were about 315 m s^{-1} and 245 m s^{-1}. The former corresponds to the Lamb mode and the latter corresponds to the Pekeris mode. The equivalent depths of these two modes estimated by using the determined phase speeds are 10.1 km and 6.1 km, respectively.

The value of the equivalent depth of the Pekeris mode determined by Watanabe, et al.

(2022) is close to that calculated by Salby (1979) but there is still a difference. Since the equivalent depth and the existence or non-existence of the Pekeris mode strongly depend on the vertical temperature profile of the atmosphere, this discrepancy may be caused by the difference between the temperature profile of USSA76 used by Salby and that of the atmosphere on the day of the Tonga eruption when the Pekeris mode was detected by Watanabe, et al. (2022). However, it is also possible that this discrepancy is due to an accuracy problem in Salby (1979)'s calculation method itself, which is discussed in the next section.

In the present manuscript, we reexamine Salby (1979)'s calculation method of the equivalent depth of the atmospheric free oscillations and propose a modifications to improve the accuracy of the calculation to determine the equivalent depth with higher accuracy. The remainder of the present paper is organized as follows. In Section 2, after we briefly review Salby (1979)'s calculation method, we propose modifications. Computational results based on the modified methods are shown in Section 3. Summary and discussion are presented in Section 4.

2. Methods

2.1 Salby (1979)'s method and its modification

The vertical structure equation and the lower boundary condition derived from the linearized primitive equations, which was solved in Salby (1979), are as follows (equation (8) in Salby (1979)).

$$\left[\frac{\mathrm{d}}{\mathrm{d}\zeta} - \frac{1}{\tilde{H}}\right]\left[\frac{1}{\tilde{H}' + \kappa}\frac{\mathrm{d}}{\mathrm{d}\zeta}(\tilde{H}Z)\right] + \alpha Z = 0, \tag{1}$$

$$\tilde{H}Z' - \kappa Z = 0 \quad (\zeta = 0). \tag{2}$$

Here, $Z(\zeta)$ is a function of the vertical structure of the pressure disturbance, and $\zeta = z/H$, where z is the geometric altitude and H is a prescribed scale height. Note that H was denoted by $\bar{H}$ in Salby (1979) but here we denote it by H to avoid confusion with $\tilde{H}$. The parameter $\kappa = (\gamma - 1)/\gamma$, where γ is the specific heat ratio, and $\alpha = H/h$, where h is the equivalent depth. Also, $\tilde{H}$ is a local scale height defined as,

$$\tilde{H}(\zeta) = \frac{R_0 \overline{T}(\zeta)}{g_0 H}. \tag{3}$$

Here R_0 is the gas constant of the dry atmosphere, g_0 is the gravity acceleration, and $\overline{T}(\zeta)$ is the vertical temperature profile of the background field. These notations are changed from Salby (1979) to be consistent with later descriptions in the present manuscript.

In Salby (1979), the vertical structure equation (1) and the boundary condition (2) were not treated as they were, but the numerical calculation was done after applying the following transform,

$$Z(\zeta) = e^{\xi/2} \tilde{H}^{-1} [\tilde{H}' + \kappa]^{1/2} v(\zeta) \tag{4}$$

and rewriting (1) and (2) as

$$v'' + k^2(\zeta; \alpha) v = 0, \tag{5}$$

$$\tilde{H} v' + \left[\frac{1}{2} - (\tilde{H}' + \kappa) + \frac{\tilde{H}\tilde{H}''}{2(\tilde{H}' + \kappa)} \right] v = 0 \quad (\zeta = 0). \tag{6}$$

(equation (11) in Salby (1979)). Here, ξ is defined as,

$$\xi(\zeta) = \int_0^{\zeta} \frac{\mathrm{d}\eta}{\tilde{H}(\eta)}, \tag{7}$$

and $k^2(\zeta; \alpha)$ is a refractive index, which is defined as,

$$k^2 = -\frac{1}{4\tilde{H}^2} + \frac{\tilde{H}'''}{2(\tilde{H}' + \kappa)} - \frac{3(\tilde{H}'')^2}{4(\tilde{H}' + \kappa)^2} - \frac{\tilde{H}''}{2\tilde{H}(\tilde{H}' + \kappa)} + \frac{\alpha(\tilde{H}' + \kappa)}{\tilde{H}}. \tag{8}$$

Note that this explicit form was not written in Salby (1979).

Salby (1979) numerically solved (5) downward starting from a sufficiently high altitude, which seems to be $\zeta = 60$ (not explicitly written in Salby (1979)), where the radiation or evanescent boundary condition was imposed, and examined how well the lower boundary condition (6) was satisfied with changing the value of α continuously. There, the background temperature profile $\overline{T}(\zeta)$ was set as described by USSA76, and the prescribed scale height H was set as,

$$H = \frac{R_0 T_*}{g_0}, \tag{9}$$

where $T_* = 250$K. This means that $H \approx 7.3$ km because USSA76 sets that $g_0 = 9.80665$ m s^{-2} and $R_0 = R^*/M_0$, where R^* is the universal gas constant which was set as $R^* = 8314.32$ kg m^2 s^{-2} K^{-1} kmol^{-1} and M_0 is the mean molecular weight at the sea surface, which was set as $M_0 = 28.9644$ kg kmol^{-1}.

In Salby (1979), it was shown that the error of (6) becomes very small (though not zero) when $\alpha = 0.764$ and $\alpha = 1.25$. The corresponding equivalent depth were $h = 9.6$ km and $h = 5.8$ km, respectively. The former corresponds to the Lamb mode, and the latter to the Pekeris mode (although the latter was called "ducted mode" there). The equivalent depth of the latter, 5.8 km, is not significantly different from the estimated value of the equivalent depth of the Pekeris mode detected in Watanabe, et al. (2022), 6.1 km. Hence, this value of the equivalent depth for the Pekeris mode obtained by Salby (1979) seems to be reasonable, but there is still a difference. Similarly, the equivalent depth for the Lamb mode obtained by Salby (1979) is also slightly smaller than the value of about 10 km estimated in many previous studies (see Sakazaki and Hamilton, 2020, and references therein). These discrepancies may, of course, be due to the fact that the realistic vertical temperature structure of the atmosphere is more or less different from that specified by the USSA76, but the calculation method of Salby (1979) has the following problem that reduces the accuracy of the numerical calculations if we examine the method.

The above mentioned problem in Salby (1979) is clearly manifested in (8) since it contains terms up to the third-order derivative of $\tilde{H}$. In the case of a background field setting like USSA76, where there is a discontinuity in the vertical gradient of temperature, $\tilde{H}''$ behaves like the δ-function and $\tilde{H}'''$ behaves like the derivative of the δ-function. This makes it very problematic to determine k^2 and to calculate it. Since the profile of $k^2(\zeta;\alpha)$ in Fig. 3 of Salby (1979) was continuously drawn, some kind of smoothing must have been done, but there was no mention of it. Also, considering the transform formula (4), it is $Z(\zeta)$ that should be continuous with respect to ζ, not $v(\zeta)$. Therefore, it is not a good idea to treat the differential equation (5) for $v(\zeta)$. Furthermore, in Salby (1979), the information on how (5) was discretized in the vertical direction and solved numerically was not written. Hence, it is difficult to reproduce Salby (1979)'s result for the error dependence on α.

To overcome the above problems, we use only the following basic transform:

$$Z(\zeta) = e^{\xi/2}\tilde{Z}(\zeta). \tag{10}$$

Then, using $\tilde{Z}$, the vertical structure equation (1) and the lower boundary condition (2) can be written as,

$$\left(\frac{\mathrm{d}}{\mathrm{d}\zeta} - \frac{1}{2\tilde{H}}\right)\left[\frac{1}{\tilde{H}'+\kappa}\left(\frac{\mathrm{d}}{\mathrm{d}\zeta} + \frac{1}{2\tilde{H}}\right)(\tilde{H}\tilde{Z})\right] + \alpha\tilde{Z} = 0, \tag{11}$$

$$\tilde{H}\tilde{Z} - \frac{\tilde{H}}{\tilde{H}'+\kappa}\left(\frac{\mathrm{d}}{\mathrm{d}\zeta} + \frac{1}{2\tilde{H}}\right)(\tilde{H}\tilde{Z}) = 0 \quad (\zeta = 0). \tag{12}$$

Now, by introducing (X, Y) as

$$X(\zeta) = \tilde{H}\tilde{Z}, \quad Y(\zeta) = \frac{1}{\tilde{H}'+\kappa}\left(\frac{\mathrm{d}}{\mathrm{d}\zeta} + \frac{1}{2\tilde{H}}\right)(\tilde{H}\tilde{Z}), \tag{13}$$

we can derive the following equations:

$$\left(\frac{\mathrm{d}}{\mathrm{d}\zeta} + \frac{1}{2\tilde{H}}\right)X = (\tilde{H}'+\kappa)Y, \tag{14}$$

$$\left(\frac{\mathrm{d}}{\mathrm{d}\zeta} - \frac{1}{2\tilde{H}}\right)Y + \frac{\alpha}{\tilde{H}}X = 0 \tag{15}$$

from (11) and (13). Then, we obtain

$$\frac{\mathrm{d}X}{\mathrm{d}\zeta} = -\frac{1}{2\tilde{H}}X + (\tilde{H}' + \kappa)Y, \tag{16}$$

$$\frac{\mathrm{d}Y}{\mathrm{d}\zeta} = -\frac{\alpha}{\tilde{H}}X + \frac{1}{2\tilde{H}}Y. \tag{17}$$

These are simultaneous ordinary differential equations for (X, Y). Using (X, Y), the lower boundary condition (12) can be expressed as,

$$X - \tilde{H}Y = 0 \quad (\zeta = 0). \tag{18}$$

As the upper boundary condition, the radiation boundary condition or the evanescent condition should be imposed. If we assume that $\overline{T}(\zeta) = T_{\mathrm{t}}(\text{constant})$ where $\zeta \geq \zeta_{\mathrm{t}}$, it follows that $\tilde{H} = \tilde{H}_{\mathrm{t}}(\text{constant})$ there. Then, from (14) and (15), we can derive the following differential equation:

$$\left(\frac{\mathrm{d}^2}{\mathrm{d}\zeta^2} - \frac{1}{4\tilde{H}_{\mathrm{t}}^2}\right)X + \frac{\alpha\kappa}{\tilde{H}_{\mathrm{t}}}X = 0 \quad (\zeta \geq \zeta_{\mathrm{t}}). \tag{19}$$

Hence, introducing q as

$$q = -\frac{1}{4\tilde{H}_{\mathrm{t}}^2} + \frac{\alpha\kappa}{\tilde{H}_{\mathrm{t}}}, \tag{20}$$

we can write the evanescent condition as

$$X(\zeta) \propto e^{-\sqrt{-q}\zeta} \quad (\zeta \geq \zeta_{\mathrm{t}}) \tag{21}$$

if $q < 0$. Also, if $q > 0$, we can write the radiation condition as

$$X(\zeta) \propto e^{-\mathrm{i}\sqrt{q}\zeta} \quad (\zeta \geq \zeta_{\mathrm{t}}) \tag{22}$$

since we can choose one of the two solutions by choosing the sign of the frequency of the disturbance without loss of generality. Because we are solving a linear homogeneous problem, there is an arbitrariness of constant multiples in the solution. Therefore, we can set as,

$$X = 1, \quad Y = \frac{1}{\kappa}\left(-\sqrt{-q} + \frac{1}{2\tilde{H}_{\mathrm{t}}}\right) \quad (\zeta = \zeta_{\mathrm{t}}), \tag{23}$$

if $q < 0$. Also, if $q > 0$, we can set as,

$$X = 1, \quad Y = \frac{1}{\kappa}\left(-\mathrm{i}\sqrt{q} + \frac{1}{2\tilde{H}_{\mathrm{t}}}\right) \quad (\zeta = \zeta_{\mathrm{t}}). \tag{24}$$

We can use either (23) or (24) as the starting condition at the point where $\zeta = \zeta_{\mathrm{t}}$, and we can solve (16) and (17) in the decreasing direction of ζ. When (X, Y) at $\zeta = 0$ is finally obtained, we can examine how well the lower boundary condition (18) is satisfied. The calculation method introduced in this subsection will be referred to as the modified Salby's method.

2.2 More sophisticated calculation

In the previous subsection, we proposed a modification to overcome the problems with the calculation method of Salby (1979). In the setting of Salby (1979), however, there was still a problem that the gravity acceleration was assumed to be constant at g_0 and the gas constant was treated as a constant (i.e., the mean molecular weight was treated as a constant), even though the altitude range above 80 km was also treated. In particular, the equivalent depth of the Pekeris mode may change if these effects are taken into account. Hence, it is necessary to examine the case where these effects are included. The vertical structure equation (1) and the lower boundary condition (2), however, were derived with assuming that the gravitational acceleration and the gas constant were constant in Salby (1979). Therefore, we will also perform the calculation using the vertical structure equation and the lower boundary condition without these assumptions. We begin with the following vertical structure equation and the lower boundary condition in the log-pressure coordinate derived from the linearized primitive equations (Andrews, et al., 1987, equation (4.2.7a) and (4.2.7b)):

$$\frac{\mathrm{d}^2 W}{\mathrm{d}\hat{z}^2} + \left(\frac{N_*^2}{g_0 h} - \frac{1}{4H^2}\right) W = 0, \tag{25}$$

$$\frac{\mathrm{d}W}{\mathrm{d}\hat{z}} + \left(\frac{R\overline{T}}{g_0 h} - \frac{1}{2}\right) \frac{W}{H} = 0 \quad (\hat{z} = 0). \tag{26}$$

Here, $\hat{z} = -H \ln(\overline{p}(\zeta)/\overline{p}(0))$ and $\overline{p}(\zeta)$ is the vertical profile of background pressure. Note that notations are changed from Andrews, et al. (1987) to be consistent with descriptions in the present manuscript. The function W represents the vertical dependence of the amplitude of the disturbance in the log-pressure coordinate through the following equation: $\mathrm{d}\hat{z}/\mathrm{d}t \propto e^{\hat{z}/(2H)} W$, where t is time. The squared log-pressure buoyancy frequency N_*^2 is written as,

$$N_*^2 = \frac{1}{H}\left(\frac{\mathrm{d}(R\overline{T})}{\mathrm{d}\hat{z}} + \frac{\kappa R\overline{T}}{H}\right). \tag{27}$$

Here, $R = R^*/M$ and M is the mean molecular weight considering altitude dependence. Note that the log-pressure buoyancy frequency differs from the usual buoyancy frequency. In addition, note also that the definition of the squared log-pressure buoyancy frequency, (27), is different from that in Andrews, et al. (1987). This form of definition is derived by considering the altitude dependence of R. See equation (6.17.23) of Gill (1982) and the explanation preceding it for details. Note, however, that the symbols are used differently.

Since the following relationship:

$$\frac{\mathrm{d}\hat{z}}{\mathrm{d}\zeta} = H^2 \frac{g(\zeta)}{R(\zeta)\overline{T}(\zeta)} \tag{28}$$

holds between $\hat{z}$ and ζ (where, $g(\zeta)$ is the gravity acceleration considering altitude dependence), we can rewrite (28) as,

$$\frac{\mathrm{d}\hat{z}}{\mathrm{d}\zeta} = \frac{H}{\hat{H}} \tag{29}$$

if we introduce $\hat{H}$ as,

$$\hat{H}(\zeta) = \frac{R(\zeta)\overline{T}(\zeta)}{g(\zeta)H}. \tag{30}$$

Hence, (25) can be rewritten in ζ-coordinate as,

$$\hat{H}\frac{\mathrm{d}}{\mathrm{d}\zeta}\left(\hat{H}\frac{\mathrm{d}W}{\mathrm{d}\zeta}\right) + \left(\frac{N_*^2 H^2}{g_0 h} - \frac{1}{4}\right) W = 0. \tag{31}$$

Also, since we can rewrite $N_*^2 H^2$ as,

$$\begin{aligned} N_*^2 H^2 &= H\frac{\overline{T}}{H}\left(\frac{\hat{H}}{H}\frac{H}{\overline{T}}\frac{\mathrm{d}(R\overline{T})}{\mathrm{d}\zeta} + \kappa R\right) = \overline{T}\left(\frac{R}{gH}\frac{\mathrm{d}(R\overline{T})}{\mathrm{d}\zeta} + \kappa R\right) \\ &= gH\frac{R\overline{T}}{gH}\left(\frac{\overline{T}}{gH}\frac{1}{\overline{T}}\frac{\mathrm{d}(R\overline{T})}{\mathrm{d}\zeta} + \kappa\right) = gH\hat{H}\left(\frac{\hat{H}}{R\overline{T}}\frac{\mathrm{d}(R\overline{T})}{\mathrm{d}\zeta} + \kappa\right), \end{aligned} \tag{32}$$

the vertical structure equation (31) can be rewritten as,

$$\hat{H}\frac{\mathrm{d}}{\mathrm{d}\zeta}\left(\hat{H}\frac{\mathrm{d}W}{\mathrm{d}\zeta}\right) + \left(\alpha\frac{g}{g_0}\hat{H}\left(\frac{\hat{H}}{R\overline{T}}\frac{\mathrm{d}(R\overline{T})}{\mathrm{d}\zeta} + \kappa\right) - \frac{1}{4}\right) W = 0. \tag{33}$$

The lower boundary condition (26) can be expressed in ζ-coordinate as,

$$\hat{H}\frac{\mathrm{d}W}{\mathrm{d}\zeta} + \left(\frac{R\overline{T}}{g_0 h} - \frac{1}{2}\right) W = 0 \quad (\zeta = 0). \tag{34}$$

Furthermore, noting that $R(0)\overline{T}(0)/g_0 = \hat{H}(0)H$ since $g_0 = g(0)$, we can rewrite (34) as,

$$\hat{H}\frac{\mathrm{d}W}{\mathrm{d}\zeta} + \left(\alpha\hat{H} - \frac{1}{2}\right) W = 0 \quad (\zeta = 0). \tag{35}$$

Similarly as the previous subsection, if we introduce V as,

$$V = \hat{H}\frac{\mathrm{d}W}{\mathrm{d}\zeta}, \tag{36}$$

we can rewrite (33) into the following simultaneous ordinary differential equations for (W, V).

$$\frac{\mathrm{d}W}{\mathrm{d}\zeta} = \frac{1}{\hat{H}}V, \tag{37}$$

$$\frac{\mathrm{d}V}{\mathrm{d}\zeta} = -\frac{1}{\hat{H}}\left(\alpha\frac{g}{g_0}\hat{H}\left(\frac{\hat{H}}{R\overline{T}}\frac{\mathrm{d}(R\overline{T})}{\mathrm{d}\zeta} + \kappa\right) - \frac{1}{4}\right) W. \tag{38}$$

Also the lower boundary condition (35) can be expressed as,

$$V + \left(\alpha \hat{H} - \frac{1}{2}\right) W = 0 \quad (\zeta = 0). \tag{39}$$

Similarly as the previous subsection, the upper boundary condition can be imposed as follows with assuming that $\overline{T}(\zeta)/M(\zeta) = (\overline{T}/M)_{\mathrm{t}}$ (constant) where $\zeta \geq \zeta_{\mathrm{t}}$ for (25) to be a differential equation with constant coefficients. Then, if we introduce $\hat{r}$ as

$$\hat{r} = \frac{1}{H^2}\left(\frac{\kappa R^*(\overline{T}/M)_{\mathrm{t}}}{g_0 h} - \frac{1}{4}\right) = \frac{1}{H^2}\left(\alpha \frac{\kappa R^*(\overline{T}/M)_{\mathrm{t}}}{g_0 H} - \frac{1}{4}\right), \tag{40}$$

we can impose the evanescent condition as,

$$W(\zeta) \propto e^{-\sqrt{-\hat{r}}\hat{z}(\zeta)} \quad (\zeta \geq \zeta_{\mathrm{t}}) \tag{41}$$

if $\hat{r} < 0$. Also, if $\hat{r} > 0$, the radiation condition can be imposed as,

$$W(\zeta) \propto e^{-\mathrm{i}\sqrt{\hat{r}}\hat{z}(\zeta)} \quad (\zeta \geq \zeta_{\mathrm{t}}). \tag{42}$$

Considering that we obtain

$$V = \hat{H}\frac{\mathrm{d}W}{\mathrm{d}\zeta} = \hat{H}\frac{\mathrm{d}\hat{z}}{\mathrm{d}\zeta}\frac{\mathrm{d}W}{\mathrm{d}\hat{z}} = H\frac{\mathrm{d}W}{\mathrm{d}\hat{z}} \tag{43}$$

from (29) and (36), we can set as,

$$W = 1, \quad V = -\sqrt{-\hat{r}}H \quad (\zeta = \zeta_{\mathrm{t}}) \tag{44}$$

if $\hat{r} < 0$. Also, if $\hat{r} > 0$, we can set as,

$$W = 1, \quad V = -\mathrm{i}\sqrt{\hat{r}}H \quad (\zeta = \zeta_{\mathrm{t}}). \tag{45}$$

We can use either (44) or (45) as the starting condition at the point where $\zeta = \zeta_{\mathrm{t}}$, and we can solve (37) and (38) in the decreasing direction of ζ. When (W, V) at $\zeta = 0$ is finally obtained, we can examine how well the lower boundary condition (39) is satisfied. The calculation method introduced in this subsection will be referred to as the sophisticated method.

The following should be added at the end of this subsection. The variable W is of a different nature than Z in the previous subsection, so their vertical profiles cannot be directly compared in the next section. The variable corresponding to variable Z is induced from W as follows (Andrews, et al., 1987, equation (4.2.6a)):

$$U = \frac{\mathrm{d}W}{\mathrm{d}\hat{z}} - \frac{W}{2H} = \frac{1}{H}\left(\hat{H}\frac{\mathrm{d}W}{\mathrm{d}\zeta} - \frac{W}{2}\right) = \frac{1}{H}\left(V - \frac{W}{2}\right). \tag{46}$$

Then, UH corresponds to Z except for constant multiples and we compare the profiles of these variables in the next section.

3. Results

3.1 Numerical results using the modified Salby's method

We integrate the simultaneous ordinary differential equations (16) and (17) for (X, Y) in the decreasing direction of ζ up to $\zeta = 0$ by using the classical 4th-order Runge-Kutta method with giving the starting point condition (23) or (24). Then we check the value of the left-hand side of the lower boundary condition (18). Here, we use the temperature profile of USSA76 (Fig. 1) as $\overline{T}$ necessary for the calculation of $\tilde{H}(\zeta)$. We set the top boundary at $\zeta_\mathrm{t} = 1000$ km$/H$ since USSA76 describes the altitude range up there. The derivative of $\overline{T}$ that is necessary to compute $\tilde{H}'$ is evaluated by the central difference as Fig. 1

$$\overline{T}(\zeta)' = \frac{\overline{T}(\zeta + \Delta\zeta) - \overline{T}(\zeta - \Delta\zeta)}{2\Delta\zeta}. \tag{47}$$

Here, we set $\Delta\zeta = 10$ m$/H$. This $\Delta\zeta$ setting is also used for the ζ decrement in the Runge-Kutta integration. Note that extrapolation based on the $\overline{T}$ definition in USSA76 is used to compute (47) at $\zeta = \zeta_\mathrm{t}$ and $\zeta = 0$. We have checked the dependence of the following results on $\Delta\zeta$ and sufficient convergence have been confirmed.

We repeat the integration with changing α continuously in the range of $0.5 \leq \alpha \leq 1.5$ and evaluate the left-hand side of (18). Figure 2 shows the dependence of $\epsilon = |(X - \tilde{H}Y)/X|$ $(\zeta = 0)$ on α. Similarly as shown by Salby (1979), there are two distinct dips but at $\alpha = 0.739$ and $\alpha = 1.107$. The corresponding equivalent depths are $h = 9.90$ km and $h = 6.61$ km, respectively. In particular, the equivalent depth corresponding to the latter Pekeris mode is significantly different from the value obtained in Salby (1979), which is considered to be because the equivalent depth of the Pekeris mode strongly depends on the vertical temperature profile of the atmosphere and is strongly affected by the calculation errors that cannot be avoided in the Salby (1979)'s calculation method.

Fig. 2

The vertical profiles of the disturbance amplitudes, $|\tilde{Z}|$, of the two modes obtained from the numerical calculations in this subsection are shown in Fig. 3. Note that the shown "amplitude" is the transformed one, $|\tilde{Z}|$, not $|Z|$. Similarly as shown in Salby (1979), the Pekeris mode (Fig. 3b) has a node in the stratosphere whereas the amplitude of the Lamb mode (Fig. 3a) decreases monotonically, almost exponentially, with altitude. Note that the node of the Pekeris mode is located at a geometric altitude of around 22.5 km in this calculation, which is lower than that obtained in Salby (1979), $3.5H \approx 25.5$ km, there. We guess that this discrepancy is a reflection of the accuracy problem with Salby (1979)'s calculation method.

Fig. 3

3.2 Numerical results using the sophisticated method

Similarly as the previous subsection, we integrate the simultaneous ordinary differential equations (37) and (38) for (W, V) in the decreasing direction of ζ up to $\zeta = 0$ by using the classical 4th-order Runge-Kutta method with giving the starting point condition (44) or (45) and examine the value of the left-hand side of (39). Numerical settings are the same as those of the previous subsection but here we take the altitude dependence of the gravity acceleration $g(\zeta)$ and the mean molecular weight $M(\zeta)$ described in USSA76 (Fig. 4). Fig. 4

Figure 5 shows the dependence of $\epsilon = |(V + (\alpha\hat{H} - 1/2)W)/W|$ $(\zeta = 0)$ on α. Although the shape of the graph is different from that of Fig. 2 due to the difference in the solved equations, there again are two distinct dips but at $\alpha = 0.739$ and $\alpha = 1.114$. The corresponding equivalent depths are $h = 9.90$ km and $h = 6.57$ km, respectively. Whereas the equivalent depth of the former Lamb mode is the same as the value obtained in the previous subsection, the equivalent depth of the latter Pekeris mode is slightly smaller than the value obtained in the previous subsection. This difference is caused by the inclusion of the altitude dependence of the gravitational acceleration and the mean molecular weight. In fact, if the equations and boundary conditions used are left unchanged and the calculations are performed with these fixed at g_0 and M_0, the positions of the dips in the $\alpha - \epsilon$ graph are exactly the same as in Fig. 2 (although the figure is not shown). Fig. 5

The vertical profiles of the disturbance amplitudes, $|W|$, of the two modes obtained from the numerical calculations in this subsection are shown in Fig. 6. Note that the shown "amplitude" here is $|W|$, not $|\tilde{Z}|$. Displaying this quantity does not change the fact that the amplitude of the Lamb mode (Fig. 6a) decreases monotonically with altitude, but for the Pekeris mode (Fig. 6b), the node is at an geometric altitude of about 10.3 km. In Watanabe, et al. (2022), it was shown that the Pekeris mode simulated by a GCM (= General Circulation Model), had a node at a pressure level of about 90 hPa (c.f. Watanabe, et al. (2022)'s Fig. 8b) with the amplitude being expressed in terms of vertical p-velocity (ω). Here, note that $\omega \propto -e^{-\hat{z}/(2H)}W$ and the node of ω should be compared with that of W. Since the pressure level of 90 hPa is at a geometric altitude of about 17 km in USSA76, the altitude of the node of the Pekeris mode determined by Watanabe, et al. (2022) is considerably higher than that determined in this subsection. This discrepancy could be due to differences in the vertical profiles of background temperatures or to some imperfection in the GCM used in Watanabe, et al. (2022).

Since the drawn profiles are for $|W|$ in Fig. 6, which does not correspond to $|Z|$ shown in Fig. 3, we cannot compare these profiles directly. Instead of $|W|$, Fig. 7 draws the profiles of $|UH|$ for U defined by (46). Comparing Figs. 3 and 7, it can be seen that although the solution methods are different, the obtained amplitude profiles of the eigenfunctions are almost identical except for constant multiples. Note also that it is natural that the altitudes of the nodes are displaced between $|W|$ shown in Fig. 6b and $|UH|$ shown in Fig. 7b, considering the continuity equation since U corresponds to the horizontal convergence. Fig. 6

The results shown in Fig. 2 and Fig. 5 are based on the geometrical altitude of the upper boundary of 1000 km, but Salby (1979) seems to set the geometrical altitude of the upper boundary at $60H \approx 440$ km. Therefore, we have done the same computations except for setting the upper boundary at 440 km, the $\alpha - \epsilon$ graph hardly changes (not shown) and the equivalent depths of the Lamb and Pekeris modes are not changed with an accuracy of three significant digits. Fig. 7

Depending on the setting of the position of the top boundary, however, perfect resonance may occur and the value of the equivalent depth may be slightly shifted. Figure 8 shows the $\alpha - \epsilon$ graph for the case where the upper boundary is set to be 91 km (the upper edge of the lowest temperature region in USSA76). In this case, the positions of the dips are at $\alpha = 0.739$ and $\alpha = 1.104$, where ϵ goes to zero. This means that a perfect resonance occurs and the Lamb mode and the Pekeris modes are exactly free oscillation modes. The reason for this perfect resonance is that the atmospheric temperature is low at 91 km, where $r < 0$, and evanescent solutions are selected. In this case, the equivalent depth of the Lamb mode remains unchanged at 9.90 km, while that of the Pekeris mode is 6.63 km. Fig. 8

From the results shown above, as long as the vertical temperature profile defined USSA76 is used, we can conclude that the equivalent depths of Lamb mode and Pekeris mode are 9.9 km and 6.6 km, respectively, with an accuracy of two significant digits if the upper boundary for the computation is above the lower edge of the thermosphere. In the present manuscript, the altitude dependence of the gravity acceleration and the mean molecular weight are taken into account. In the thermosphere, the specific heat ratio γ should also change with height, but this is not taken into account (In USSA76, only the information that $\gamma = 1.4$ is given, and the altitude dependence of γ is not described). However, considering the fact that the equivalent depths of the Lamb and the Pekeris modes did not change between the above calculations with setting the upper boundary at 1000 km and that with setting the upper boundary at 440 km (even though the mean molecular weight is nearly 5 times different at those two altitudes), it is considered that even if the dependence of γ on the altitude is given accurately, it will not affect the calculation of equivalent depth.

4. Summary and Discussion

In the present manuscript, we re-examined the calculation of Salby (1979) in relation to the Pekeris mode, which was firstly detected by Watanabe, et al. (2022) from observations of waves generated by the eruption of Tonga, in order to examine what its equivalent depth value would be under a standard vertical atmospheric temperature profile such as USSA76. After examining the calculation of Salby (1979), it was found that the transformation of the equation there was inappropriate for the case where there is a discontinuity in the vertical temperature gradient, such as USSA76. Therefore, in the present manuscript, we presented an improved calculation method and calculated the equivalent depths for the

Lamb and the Pekeris modes. In addition, several calculations were performed for different position settings for the upper boundary, taking into account the altitude dependence of the gravity acceleration and mean molecular weight, which were not taken into account in Salby (1979). It is concluded that the equivalent depth values obtained in Salby (1979) are incorrect, and that under the atmospheric temperature profile of USSA76, the equivalent depths of the Lamb and the Pekeris modes are 9.9 km and 6.6 km, respectively, in two significant digits (The equivalent depth of the Pekeris mode varies slightly depending on the setting of the position of the upper boundary, but does not change within the range of two significant digits).

The equivalent depth of 6.6 km for the Pekeris mode obtained in the present manuscript is larger than that of 6.1 km estimated from the observation of waves generated by the eruption of Tonga in Watanabe, et al. (2022). There seem to be two main reasons for this discrepancy: first, the USSA76 vertical temperature profile used in the present manuscript is for midlatitudes, which may be different from the vertical temperature profile at the latitudes where the Pekeris mode was excited and where it propagated by the time used to determine its phase velocity; second, Watanabe, et al. (2022) estimated the phase velocity of waves from observations, it is possible that the phase velocity can differ from that of the stationary atmosphere due to background winds. We should also note here that, in Watanabe, et al. (2022), they also conduced a spectral analysis of 57 years of hourly global reanalysis data and showed that there was a distinct spectral peak corresponding to the Pekeris mode (Watanabe, et al. (2022)'s Fig. 9d), but the corresponding equivalent depth for the spectral peak seemed to be larger than 6.1 km. This may imply that the long-term climatological value of the equivalent depth of the Pekeris mode may be close to the value determined in the present manuscript, 6.6 km. In order to investigate which of the above mentioned reasons may be responsible for the discrepancy between the equivalent depth of the Pekeris mode obtained in the present manuscript and that estimated by Watanabe, et al. (2022), the first step would be to calculate the equivalent depth using the present method, given the horizontally averaged vertical temperature profile of the atmosphere at the time of Tonga's eruption, which will be our next work.

Supplements and Data Availability Statements

Supplement 1 is a Fortran90 program which computes the α dependence of ϵ shown in the present manuscript. The terms and conditions of the program are subject to the JMSJ Submission Regulation.

All data analyzed in this study are generated by this program.

Acknowledgments

We thank Dr. Takatoshi Sakazaki, two anonymous reviewers, and the journal editors for their helpful comments. Special thanks to one of the reviewers for pointing out a serious error in the original version of the manuscript. This work was supported by JSPS KAKENHI Grant Numbers 20K04061.

The GFD-DENNOU Library (http://www.gfd-dennou.org/arch/dcl/) was used to draw the figures.

References

Andrews, D. G., J. R. Holton, and C. B. Leovy, 1987: *Middle atmosphere dynamics.* Academic press, 489pp.

Gill, A. E., 1982: *Atmosphere-ocean dynamics.* Academic press, 680pp.

NOAA, NASA, and USAF, 1976: *U.S. STANDARD ATMOSPHERE, 1976*. U.S. Government Printing Office, 227pp.

Pekeris, C. L., 1937: Atmospheric oscillations. *Proceedings of the Royal Society of London*, **A158**, 650–671.

Sakazaki, T. and K. Hamilton, 2020: An array of ringing global free modes discovered in tropical surface pressure data. *Journal of the Atmospheric Sciences*, **77**, 2519–2539.

Salby, M. L., 1979: On the solution of the homogeneous vertical structure problem for long-period oscillations. *Journal of the Atmospheric Sciences*, **36**, 2350–2359.

Watanabe, S., K. Hamilton, T. Sakazaki, and M. Nakano, 2022: First Detection of the Pekeris Internal Global Atmospheric Resonance: Evidence from the 2022 Tonga Eruption and from Global Reanalysis Data. *Journal of the Atmospheric Sciences*, *Early Online Release*, https://doi.org/10.1175/JAS-D-22-0078.1.

List of Figures

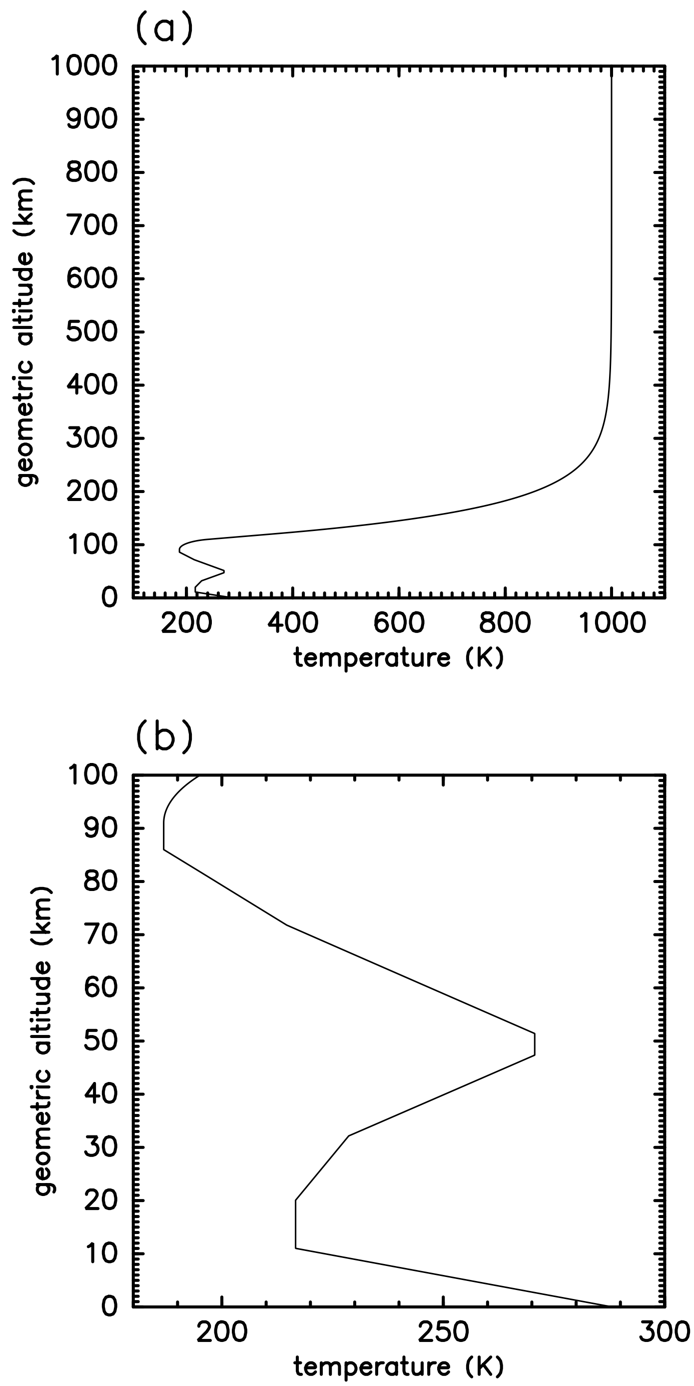

Fig. 1. Vertical temperature profile described in USSA76. (a): temperature profile up to 1000 km. (b): temperature profile up to 100 km.

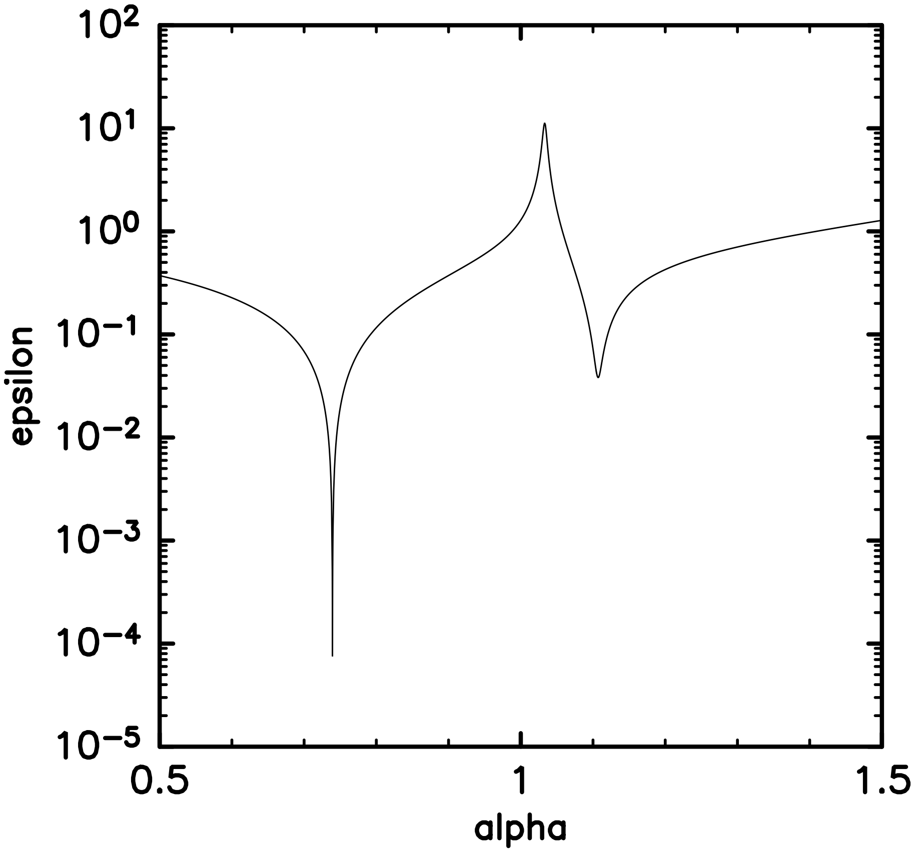

Fig. 2. Dependence of the error (ϵ) of the lower boundary condition on the parameter $\alpha = H/h$. The computation is done by using the equations in Section 2.1 and setting the top boundary at 1000 km.

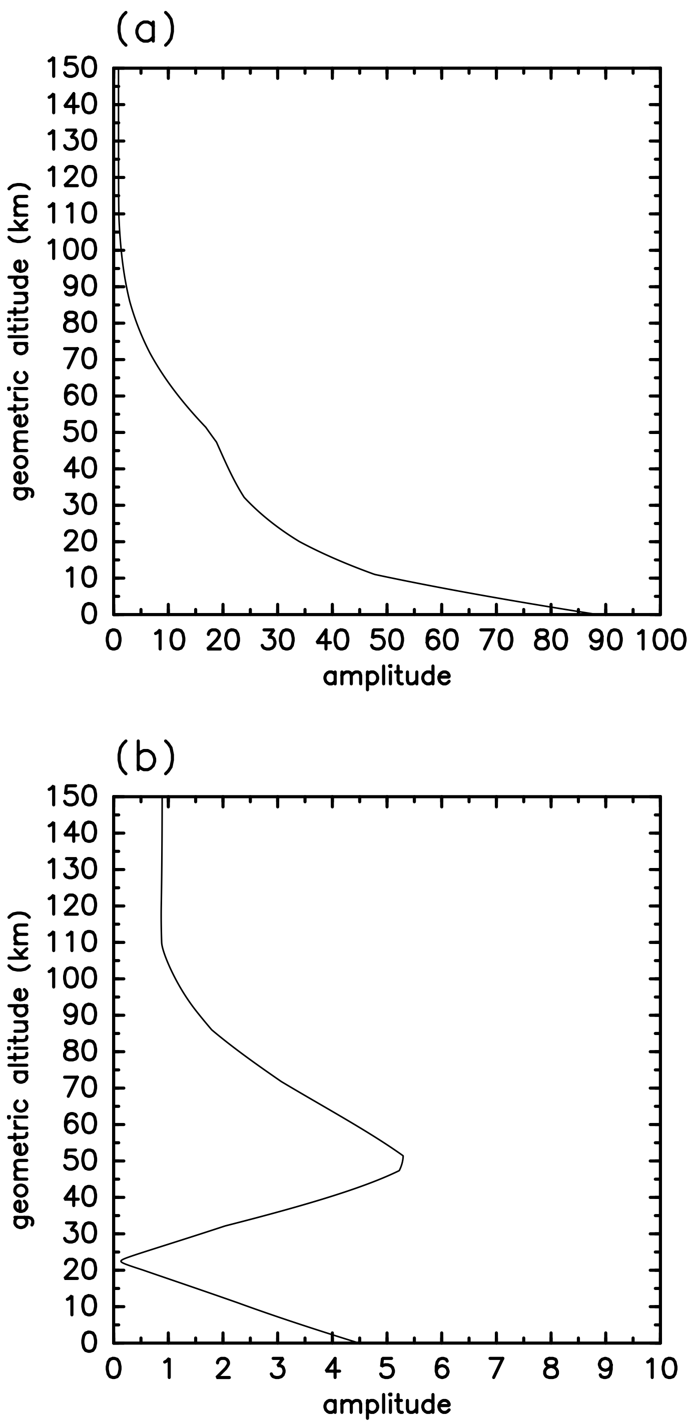

Fig. 3. Vertical profiles of the amplitudes, $|\tilde{Z}|$, of the two modes obtained in Section 3.1. (a): case for $\alpha = 0.739$ ($h = 9.90$km). (b): case for $\alpha = 1.107$ ($h = 6.61$km).

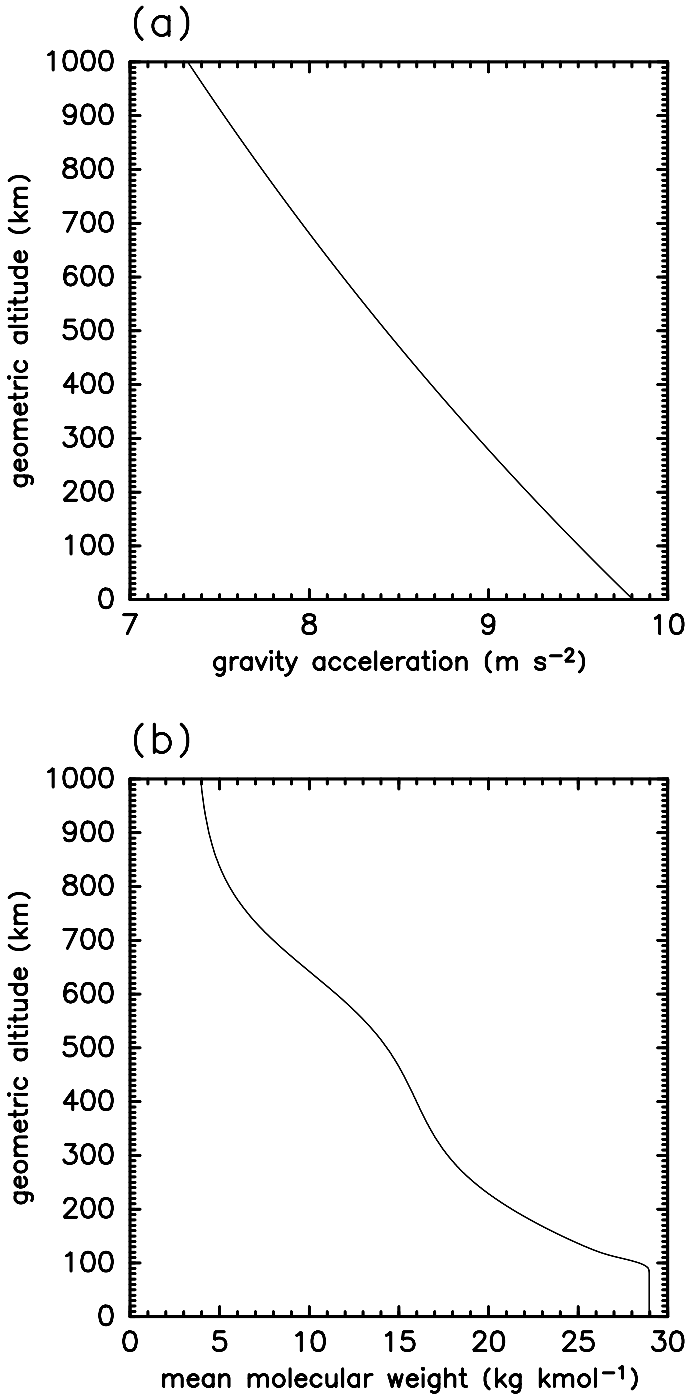

Fig. 4. Vertical profiles of the gravity acceleration and the mean molecular weight described in USSA76. (a): gravity acceleration. (b): mean molecular weight.

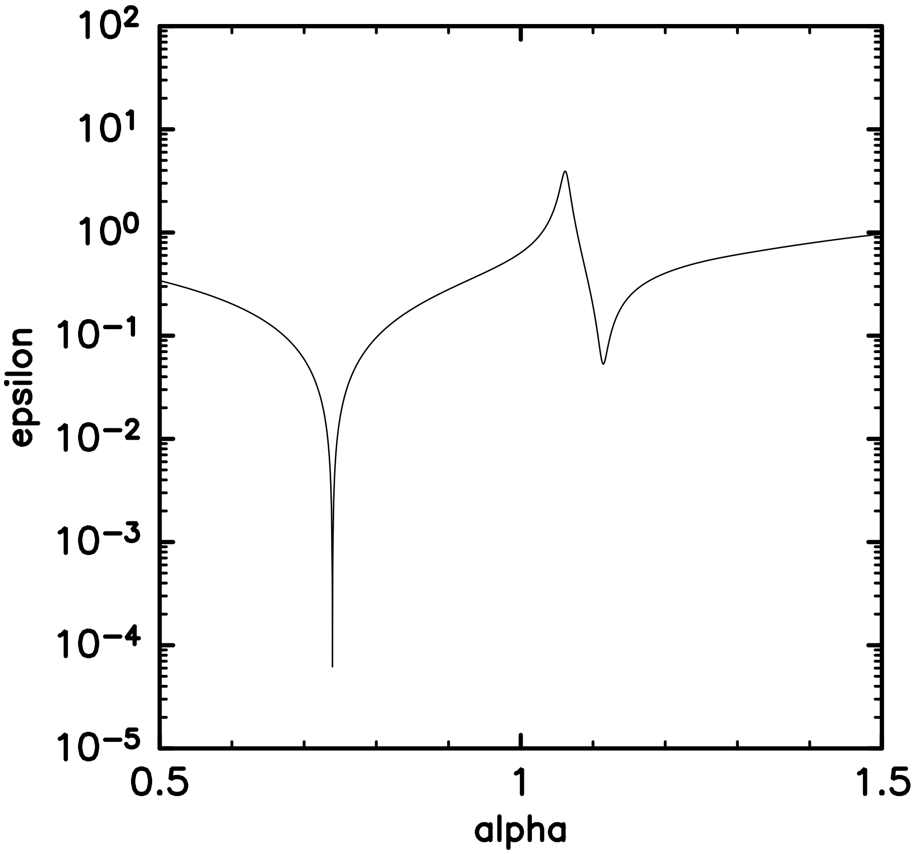

Fig. 5. Same as Fig. 2 except that the computation is done by using the equations in Section 2.2.

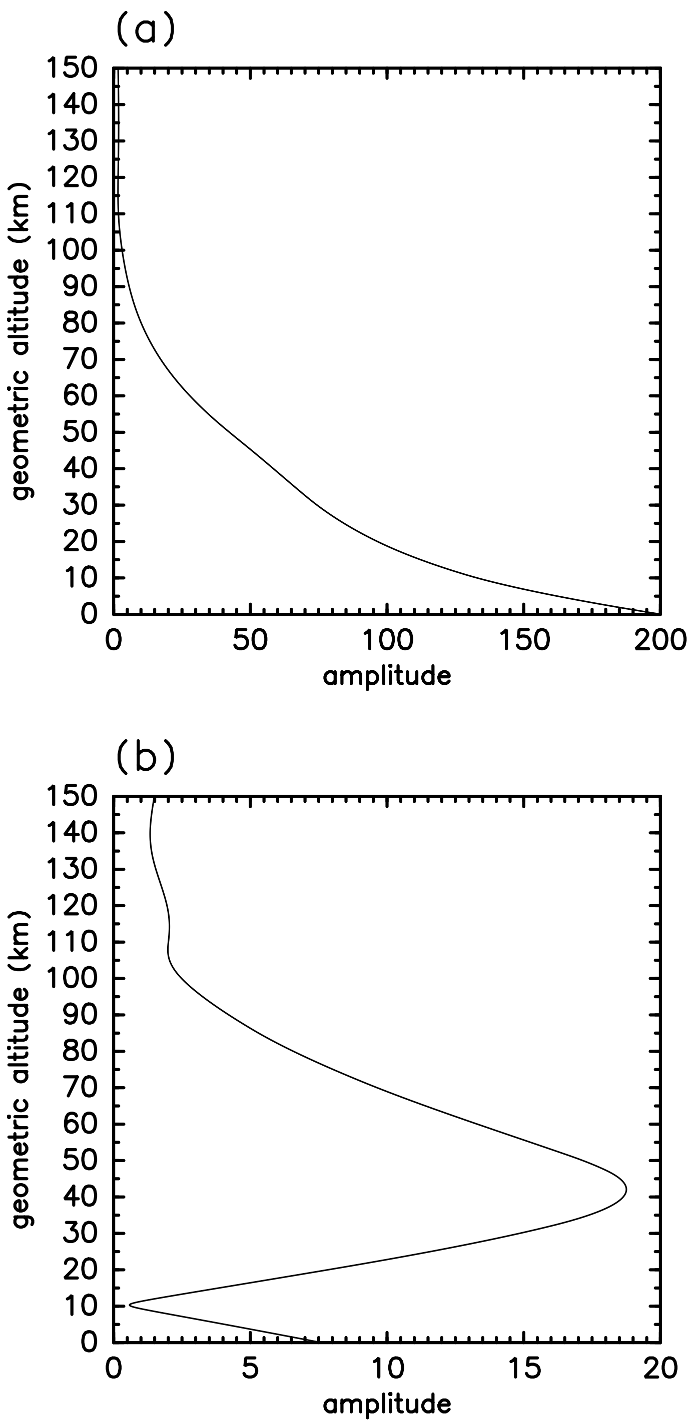

Fig. 6. Vertical profiles of the amplitudes, $|W|$, of the two modes obtained in Section 3.2. (a): case for $\alpha = 0.739$ ($h = 9.90$km). (b): case for $\alpha = 1.114$ ($h = 6.57$km).

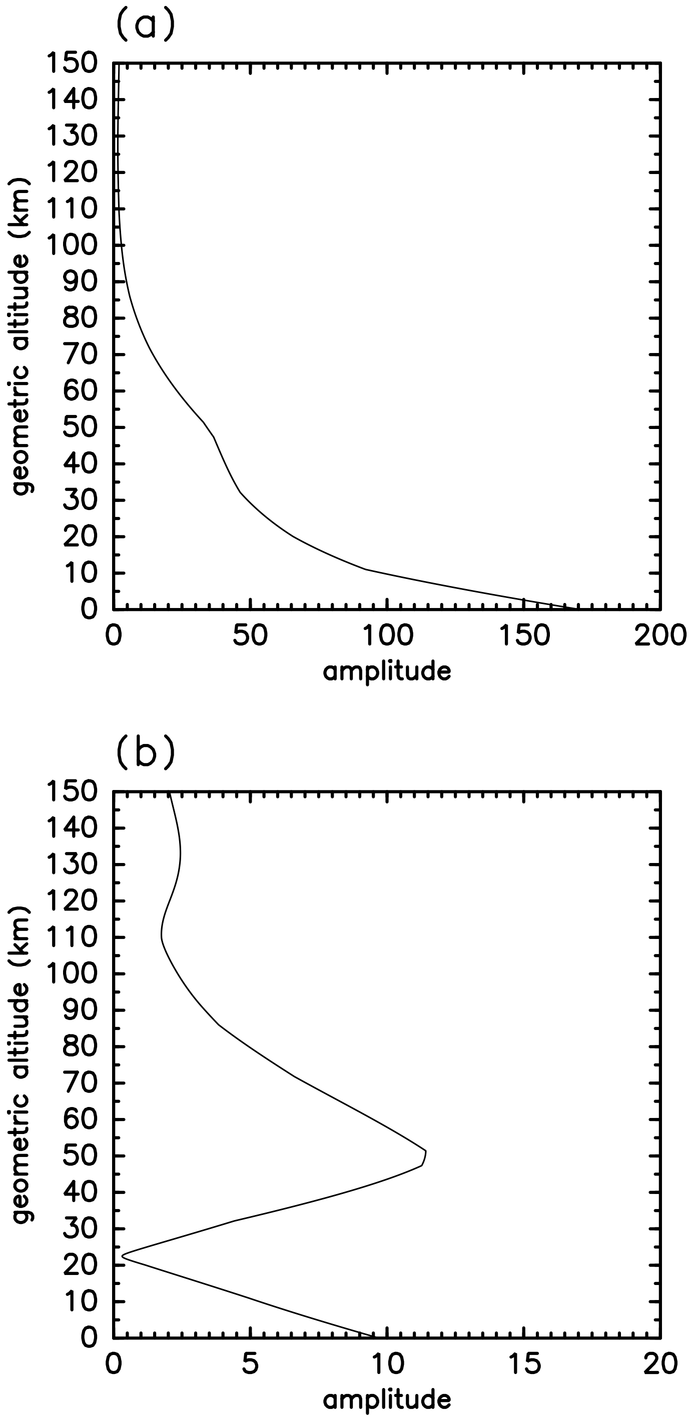

Fig. 7. Vertical profiles of the amplitudes, $|UH|$, of the two modes obtained in Section 3.2. (a): case for $\alpha = 0.739$ ($h = 9.90$km). $\alpha = 1.114$ ($h = 6.57$km).

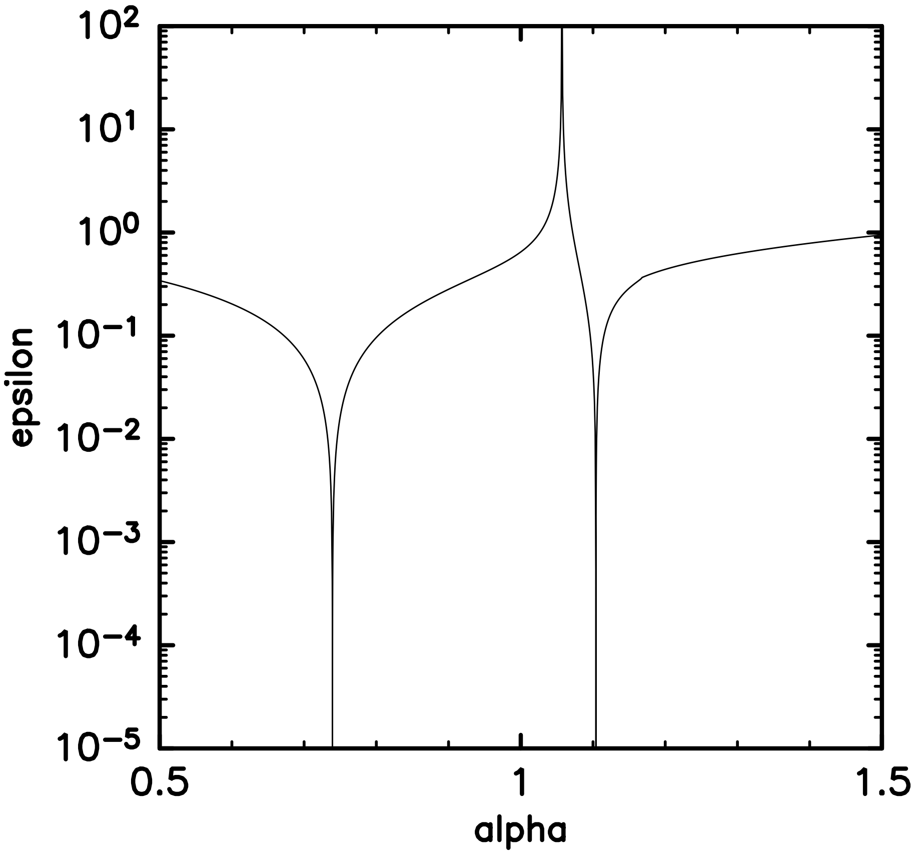

Fig. 8. Same as Fig. 5 except that the computation is done by setting the top boundary at 91 km.